Regulative Characteristic of Methanol-Copper Heat Pipes for Asteroid Lander "MASCOT"

Volodymyr Baturkin[1]
German Aerospace Center (DLR), Institute of space systems
Department "Mechanics and Thermal Systems"
Robert-Hooke-Str. 7, Bremen, 28359, Germany
email: volodymyr.baturkin@dlr.de

Vitali Feidelheimer
FH Aachen, University of Applied Sciences
Faculty of Aerospace Engineering
Hohenstaufenallee 6, Aachen, 52064, Germany
email: vitali.feidelheimer@alumni.fh-aachen.de

Kaname Sasaki
German Aerospace Center (DLR), Institute of space systems
Department "Mechanics and Thermal Systems"
Robert-Hooke-Str. 7, Bremen, 28359, Germany
email: kaname.sasaki@dlr.de

Eugen Mikulz
German Aerospace Center (DLR), Institute of space systems
Department "Mechanics and Thermal Systems"
Robert-Hooke-Str. 7, Bremen, 28359, Germany
email: eugen.mikulz@dlr.de

Tra-Mi Ho
German Aerospace Center (DLR), Institute of space systems
Department "System Development and Project Office"
Robert-Hooke-Str. 7, Bremen, 28359, Germany
email: tra-mi.ho@dlr.de

ABSTRACT

Variable conductance heat pipes (VCHPs) are the main part of the MASCOT (Mobile Asteroid surface SCOuT) lander thermal control system (TCS). They provide variable conductivity by utilizing the heat transfer limitations. This allows the heat pipes to act as thermal switches without additional constructive

[1] – corresponding author

elements, thus leveraging the simple and compact design of conventional heat pipes. Two cylindrical methanol-copper heat pipes with shell length of 0.482 m and 0.438 m and external diameter of 0.006 m, having copper discrete metal fiber wick and copper shell were constructed and verified in the temperature range between −75 and +60 °C. The purpose is to apply this design into the MASCOT thermal control system and to investigate the heat pipes' regulative characteristics and heat transfer limitations. VCHPs show a change of thermal resistivity from 70 K/W at a heat sink temperature of −60 °C, to 0.8 K/W at a heat sink temperature of +60 °C; with an obtained maximal heat transfer rate of 5 W and 16 W, respectively. It is found that the switching effect of the heat pipes is governed by the sonic velocity limitation, the saturation vapor pressure of the working fluid and the maximal capillary pressure of the wick. The operation of the heat pipes as the part of the TCS has confirmed their variable thermal properties.

Keywords: heat pipes; cooper-methanol; metal fiber wick; heat transfer limitations; variable conductance

1 INTRODUCTION

MASCOT is a surface science package which was developed as an asteroid explorer of 10 kg for the asteroid sample return mission Hayabusa2 (HY2). Since December 2014, it was flying piggyback onboard the HY2 spacecraft and landed after nearly 4 years of cruise on the near-Earth asteroid (162173) Ryugu [1] in October 2018. MASCOT performed in-situ investigation of the asteroid with its four science instruments: a camera 'MASCAM' [2], a near-IR hyperspectral microscope 'MicrOmega' [3], a magnetometer 'MASMAG' [4] and a radiometer 'MARA' [5].

The MASCOT Thermal Control System (TCS) has to assure that all subsystems and payloads are in dedicated temperature ranges over the whole mission lifetime. This is realized by a delicate design of thermal interfaces between different components [6],

the most important interface of which is the connection between the electronic box and the radiator. The main components of the lander, including thermal interfaces and heaters, are described in Fig. 1. A major challenge of the MASCOT TCS design is to satisfy diverse thermal requirements in different mission phases. During the cruise phase of the HY2 spacecraft and its asteroid proximity operation, the power of MASCOT is nominally off, except for periodic MASCOT in-flight operations. Only the survival heaters of the lander are constantly powered by HY2. Regarding its thermal environment, the MASCOT lander is shadowed by the HY2 high gain antenna and the solar panel. Considering the possible conductive and radiative interface temperature variation between −20 and +60 °C, the heat exchange between MASCOT and HY2 is required to be within ±5 W. During this phase, the lander's subsystems and payloads have to stay within their non-operational temperature limits, whereas the battery pack as one of the most temperature sensitive equipment has to be maintained around −30 °C.

When MASCOT is operated for health checks and payload calibrations, the TCS shall provide the corresponding operational temperatures for all subsystems and payloads. Before every switch-on, a dedicated MASCOT pre-heating operation, which is realized by a setting change of the survival heaters, is performed. During these phases, the TCS of MASCOT should limit the heat exchange with HY2 and with the external environment, in order to satisfy the interface requirement and to use the survival heaters efficiently.

Contrary to the cruise phase and the asteroid proximity operation, MASCOT is subject to a dynamic thermal environment once landed on the asteroid. In order to

deliver MASCOT to the asteroid surface, HY2 firstly descends from its home position at 20 km towards the asteroid. During this phase, MASCOT receives increasing thermal radiation from the asteroid. At an altitude of 60 m, the lander is separated from the HY2 spacecraft, starts freefall to the asteroid's surface, and bounces on the surface until it reaches a settled condition. In this phase, the heat flux of the Sun and the asteroid flows into the side walls of the lander. MASCOT experiences large variations of the solar flux and the asteroid surface temperature, because of the day and night transition of the asteroid. Under this dynamic thermal environment, the lander performs intensive payload operations. Therefore, during the on-asteroid phase, the TCS has to efficiently reject the generated heat through the radiator at day time, and to insulate the electronic equipment from overcooling at asteroid night.

After a trade-off study of the MASCOT TCS design, a methanol-copper heat pipe was selected as the heat transfer component between the electronic box and the radiator. This type of heat pipes has an external shape of constant conductance heat pipes, but its thermal performance is similar to that of variable conductance heat pipes [7]. Such type of heat pipes has space flight heritage, since it has been used in several projects, such as SKALA (1980), Fragment (1983) and Magion-4&5 (1995, 1996) [8]. These heat pipes operated at heat sink temperature between −10 and +50 °C, and transferred heat power from 2 to 20 W. The minimal to maximal thermal resistance varied from 1.2 K/W to 8 K/W.

The mechanism of variable heat transfer in methanol-copper heat pipes is connected with large variation of thermophysical properties of methanol, which causes

different operational regimes of the heat pipe operation. In some regimes the heat pipes operate with limited vapor and liquid circulation between the condenser and the evaporator. Such conditions are not desirable for conventional heat pipes. In this paper, we present a more detailed study of the operation of the methanol-copper heat pipe, focusing on their variable thermal properties.

Two methanol-copper heat pipes with a sintered metal fiber wick were examined. They are the two-dimensional versions of the three-dimensional heat pipes integrated in the MASCOT lander [9]. The heat pipe type A (HP-A) has four curvatures (2 × 90° and 2 × 120°) and the heat pipe type B (HP-B) has five curvatures (2 × 156° and 3 × 90°), as shown in Fig. 2 and Table 1. The goal of this study is to understand the heat transfer limitation effect on the variable characteristics of methanol-copper heat pipes.

2 LIMITING FACTORS OF HEAT TRANSFER

The investigated methanol-copper heat pipes are designed to operate in a temperature range between −80 and 120 °C. In this range, they are subject to several heat transfer limitations. During the design of a heat pipe, the calculation and the knowledge of the occurrence of limitations are essential. For conventional design, the primary objective is to avoid operation in the limiting regime to guarantee the best performance. Faghri [10] has summarized the occurrence of heat transfer limitations as a function of the operating temperature (or saturation pressure / temperature) and the heat input. Figure 3 shows this relation qualitatively, indicating that the limitations have transition zones where they interact together. However, in the analytical calculation

they are treated individually with no perturbations and are only valid for steady state in the operating domain. This domain is below the line of any limitation which may be encountered first. But heat pipes operating above the calculated limitations are subject to a more complicated state. The nearly isothermal behavior of a heat pipe does not exist anymore and a definition of an operating temperature is not straightforward. A temperature difference between evaporator and condenser can be more than 100 K. From the analytical calculation it is impossible to identify the acting limitation, or a combination of them. However, exactly this behavior is desired by a VCHP. It separates the cold heat sink from the hot operating payload. The identification of the heat transfer limitations that cause the variable conductance of the methanol-copper heat pipes with fibrous capillary structure is the primary objective.

For the calculation of the heat transfer limitations, a custom-made methanol thermophysical properties database is developed. This is necessary since there is no reference including all required thermophysical properties. Especially for temperatures below −40 °C, the properties spread up to 20 % between the used sources. These properties are calculated by the temperature ratio $T_r = T/T_{\mathrm{CRI}}$, where the critical temperature $T_{\mathrm{CRI}} = 512.5\ \mathrm{K}$, and the temperature of interest is *T*. The polynomial is defined by Eq. (1)

$$f(T) = \sum_{i=0}^{1\ldots3} A_i \cdot T_r^i \tag{1}$$

where $f(T)$ is the sought property in SI units and A_i is a coefficient of the polynomial. The coefficients are given in Table 2 with validity between −80 and 150 °C. Subscript "l" is used for liquid and "v" - for vapor.

From the shown heat transfer limitations in Fig. 3, the following limitations can be excluded. (1) - the continuum flow limitation is only of concern for vapor flow in the rarefied condition. Investigation of the Knudsen number **Kn** for these heat pipes shows a maximal Knudsen number of $\mathbf{Kn}_{\max} = 0.23$ at a saturation temperature of −80 °C, which is in the region of slip flow. Therefore, the heat pipes are at no point in rarefied flow conditions. Continuum flow condition is fully established at a saturation temperature of −51 °C ($\mathbf{Kn} = 0.01$). (2) - the frozen start up limitation is a subject of high temperature heat pipes starting from a frozen state. The used working fluid methanol has a melting point at −97.6 °C, which is below the operational temperature. (3) - the condenser limitation is reached when the heat sink is not able to reject the applied heat. This is never the case for this study. The heat rejection rate is higher than the applied heat. Further, this limitation can only be reached when all the other limitations are not encountered, which is never the case for these heat pipes. (4) - even though the heat pipes operate above the boiling point of methanol (+64.7 °C), the boiling limitation for heat pipes with metal fiber wick is not a limiting factor but the fundamental operational mode as pointed out by Semena [11].

The remaining limitations are the viscous, sonic, entrainment and capillary limitations. The viscous and sonic limitations are connected with the vapor flow and low saturation temperatures. The capillary limitation is mainly connected with the liquid flow. The entrainment limitation is a function of the vapor flow velocity and the surface tension of the liquid phase. These four limitations are described in more detail below.

2.1 Viscous Limitation

In the viscous limitation, the heat pipes operate near the triple point with low saturation pressure. The heat transfer is limited because of the viscous pressure losses in the vapor flow and the reduced maximal possible pressure drop. Busse [12] made an analytical approach to identify the viscous limitation. Taking the assumption of a laminar flow of isothermal perfect gas, the limitation can be described by Eq. (2)

$$Q_{v,\max} = \frac{A_v d_v^2 H_{fg} \rho_0 p_0}{64 \mu_v L_{\mathrm{Eff}}} \left(1 - \frac{p_{L_T}^2}{p_0^2}\right) \tag{2}$$

With the maximal possible vapor pressure drop, by taking $p_{L_T} = 0$ at the condenser endcap and $p_0 = p_{\mathrm{sat}}$ and vapor density ρ_0 and viscosity μ_v at the evaporator endcap, the viscous limitation can be calculated. This assumption is made by Busse [12] and Faghri [10]. It may hold for heat pipes with a low maximal capillary pressure compared to the saturation pressure. But, for the investigated low temperature methanol heat pipes, neglecting the liquid pressure drop in Eq. (2) yields to an error in $Q_{v,\max}$ definition to 134 % at an evaporator endcap temperature of −40 °C and to 225 % at the transition point of −27 °C.

An alternative approach is presented by taking the liquid pressure drop additionally into account. Since the heat pipe is a closed system, the sum of the liquid and vapor pressure drop cannot exceed the maximal occurring pressure in the evaporator. At low temperatures, the maximal pressure drop is limited by the saturation pressure. As example for a temperature of −40 °C at the evaporator endcap and a heat input power of 0.4 W, the total pressure drop in liquid and in vapor is 200 Pa and the liquid friction part is 170 Pa. Saturation vapor pressure is as well 200 Pa. The viscous limitation is inhibiting the heat transfer as long as the saturation pressure p_{sat} is lower

than the maximal capillary pressure drop $\Delta p_{c,\max}$. When the saturation pressure is higher than the maximal capillary pressure, the heat pipe is limited by the capillary pressure. By taking the liquid pressure drop into account, the viscous limitation can be described with Eq. (3)

$$Q_{v,\max} = \frac{p_{\text{sat}} H_{fg}}{\left(\frac{\mu_l}{\rho_l A_w K} + \frac{8\mu_v}{\pi r_v^4 \rho_v}\right) L_{\text{Eff}}} \tag{3}$$

where the first term in the denominator describes the liquid pressure drop and the second describes the vapor pressure drop. This formulation is similar to that of the capillary limitation, but with the saturation pressure as a reference. To calculate the viscous limitation, the reference temperature for the thermophysical properties is taken at the endcap's outer edge of the evaporator. In the test setup, the first temperature sensor on the evaporator flange was used as a reference. For all technical purpose, these two temperatures are considered to be equal.

2.2 Sonic Limitation

The sonic limitation appears after the viscous limitation and is a thermodynamic barrier. In a heat pipe, the vapor flow may reach a Mach number of unity **M** at the evaporator outlet or with an adiabatic section at the transition to the condenser section. This condition is reached when the heat pipe operates at high heat inputs or low vapor density. A similarity exists between a convergent-divergent nozzle and a heat pipe. Kemme [13] was the first noting this. In a convergent-divergent nozzle, the fluid flow can reach maximal Mach number of unity at the throat. This is known as the choked flow condition. A heat pipe has no convergent section, the similarity origins from the

mass addition at the evaporator. Analytical approximation of the sonic limitation can be made with the assumptions that the flow is one-dimensional, compressible, frictionless, perfect gas. Three analytical approaches are made with further assumptions, that the flow is isothermal, derived by Busse [12]; or that the flow is isentropic, derived by Levy [14]. The third attempt is made by Bertossi et al. [15] considering the saturated vapor flow. This analysis takes the evolution of the thermophysical properties on the saturation curve into account, since they do not follow the ideal gas law. Only low practical impact on the calculated sonic limitation can be found, comparing the three approaches together. In the analysis of these heat pipes, the vapor flow is investigated by methods of Computational Fluid Dynamics (CFD). The heat pipes are modelled in a 2D-axisymmetric coordinate system with structured quadrilateral mesh, having about 63300 elements. For the simulation, the vapor flow and heat conduction in the shell, wick and vapor space are considered. The vapor flow is considered laminar and compressible; the corresponding Navier-Stokes equations are solved using the direct solver PARDISO of COMSOL which uses the Newton method with automatically adapted damping factor. Heat transfer between wall and vapor is described by linear heat conductivity equation. For the fully saturated wick, an experimental value of effective heat conductivity is used [11]. The heat transfer in vapor is coupled with the obtained velocity field. The simulation is terminated when the relative error is below $1x10^{-6}$. As a boundary condition for the vapor flow, the saturation temperature at the liquid-vapor interface is used as basis to calculate the saturation pressure p_{sat} using the methanol database (Table 2). The vapor is driven by a pressure drop between the evaporator and

condenser, which is the result of a temperature difference between both. To simulate the evaporation and condensation process a heat source is added at the liquid-vapor interface in the evaporator and the condenser which is dependent on the mass in and out flow. Steady-state is considered. In this case the amount of evaporated heat is the same as for condensed. For all inner walls, the no-slip boundary condition is applied. At the condenser, a convective boundary condition with forced convection is used. The result is the velocity field and pressure drop along the heat pipe.

It is found that for the average condenser temperature below −60 °C sonic flow condition is reached at about −42 °C at the evaporator endcap. Lowering the condenser temperature does not affect the occurrence, due to small variation of the saturation pressure in the condenser. For a condenser temperature of −50 °C it is reached at −26 °C at the evaporator endcap, for −40 °C at −20 °C and for −30 °C at −9 °C, respectively. Above an operation temperature of −27±2 °C the heat pipe is dominated by the capillary limitation.

2.3 Capillary Limitation

The capillary limitation is reached when the sum of the liquid and vapor pressure drop is higher than the maximal occurring capillary pressure. For a heat pipe with a metal fiber wick the maximal capillary pressure is defined by Eq. (4)

$$p_{c,\max} = \frac{35\sigma}{d_f}(1-\varepsilon)\sqrt{1-\exp\left(-\frac{6d_f}{l_f}\right)} \tag{4}$$

with d_f and l_f as fiber diameter and length, respectively [16]. Taking the maximal capillary pressure from Eq. (4) the hydrodynamic limitation can be described with Eq. (5)

$$Q_{c,\max} = \frac{p_{c,\max} H_{fg}}{\left(\frac{\mu_l}{\rho_l A_w K} + \frac{8\mu_v}{\pi r_v^4 \rho_v}\right) L_{\mathrm{Eff}}}. \quad (5)$$

This limitation dominates the operation of the heat pipe at temperatures above −27±2 °C. The transition point at this temperature is defined by the condition $p_{c,\max} = p_{\mathrm{sat}}$. For $p_{c,\max} \geq p_{\mathrm{sat}}$, the heat pipe is dominated by the viscous limitation and for $p_{c,\max} \leq p_{\mathrm{sat}}$ by the capillary.

2.4 Entrainment Limitation

The liquid and vapor are counter flows interacting together at the liquid-vapor interface. The shear stress causes the liquid to entrain the vapor flow. The liquid droplets are carried back toward the condenser section forming a liquid slug at the endcap. This phenomenon creates shortcut of the liquid return path, causing a faster dry-out at the evaporator accompanied by the capillary limitation. Kim et al. [17, 18] made experimental and mathematical analysis of the entrainment limit of a heat pipe with water as working fluid. In total, they found twelve different models predicting the occurrence of the entrainment limit. In their analysis they identified critical Weber number $\mathbf{We_{CRI}}$ between 0.2 and 10. The expression of the entrainment limitation as made by Faghri [10] or Kim et al. [17, 18] does not provide an accurate estimation. A proper analytical description of this limitation is impossible as all models predicting this limitation depend on empirically found parameters. Nevertheless, this limitation has its eligibility and must be considered as one limiting factor. The calculated heat transfer limitations for HP-A are shown (similar for HP-B) in Fig. 4.

These limitations are identified to be responsible for the variable conductance of MASCOT's heat pipes. At a mean temperature of about −27±2 °C in the evaporator, a transition between the viscous to the capillary limitation occurs. The sonic limitation is above the viscous limitation calculated with Eq. (3). These two limitations are working together. For example, when the mean condenser temperature is −60 °C the sonic limitation is reached at an evaporator endcap temperature of −42 °C. At this point, the heat pipe is in choked flow condition. But the maximal saturation pressure still dominates the heat transfer limitation since it is lower than the maximal capillary pressure until an average temperature of −27±2 °C is in the evaporator.

3 EXPERIMENTAL SETUP

All tests were carried out at the DLR Institute of Space Systems in the thermal vacuum chamber SSA with a volume of 0.8 m^3 in a pressure environment below 10^{-6} mbar, avoiding convective heat transfer. Figure 5 shows the test set up inside the thermal vacuum chamber. The heat pipes (1) are fixated on the condenser block (2) and the evaporator stands (3).

A thermal insulation (4) prevents heat transfer from the temperature support plate (8) to the evaporator. For a uniform temperature environment, a thermal compartment is realized with a copper shroud (5) covering this plate. To have a uniform radiation inside the shroud, a single layer insulation (SLI) is attached to its inner walls. Outside, to minimize the temperature exchange, the mounting plate and shroud are covered with multi-layer insulation (MLI) (6). The plate stands on four alignment screws

(7) on a wagon (10) made of aluminum profiles. They are used to level the mounting plate. The height difference between evaporator and condenser was measured by two calibrated Seika NBA3 inclination sensors (x and y tilts). The heat sink temperature (mounting plate) is regulated with a liquid cryostat Huber 385 (Chiller). The heater for each heat pipe consists of flexible film resistors, glued to a 0.002 m thick copper substrate which is attached to the heat pipe flange. The heaters are operated with power supply HAMEG HP4040.

The measurement system YOKOGAWA DC100 (DAQ) and twelve custom-made PT100 sensors with constantan wires record the temperature along the heat pipe shell (system accuracy of 0.05 K). They are uniformly distributed in the evaporator flange (4 units), the adiabatic section (4 units) and the condenser section (4 units). The power supply HAMEG HP4040 is remote controlled with LabVIEW for powering the flat film heaters, installed on the flat copper substrate, and recording voltage, current and power values. The heaters were operated in a constant voltage mode. The liquid thermostat and the DAQ were accessed via the vendor software. SEIKA NBA3 inclination sensors and the power supply system were integrated in a LabVIEW environment to enable cross-communication and full automatic testing. Inside the DLR network the Windows tool “Remote desktop” was used to remote control the testing computer. The access from outside was realized via a Virtual Private Dialup Network (CISCO).

4 ACHIEVEMENT OF VARIABLE CONDUCTANCE CHARACTERISTICS

A steady state test was conducted to get the regulative characteristics of the heat pipes, therefore a constant temperature is held at the heat sink. The heat input is

increased after steady state is reached in the evaporator (<0.2 K/h). The test is conducted for heat sink temperatures from −70 to +60 °C and heat inputs of 0.5 W to 16 W. Figure 6 shows the change of the thermal resistance of HP-A, which is calculated by dividing the difference between the mean evaporator temperature and the mean condenser temperature by the applied power. Both heat pipes show a change of thermal resistivity from about 70 K/W at a heat sink temperature of −70 °C, to 0.8 K/W at a heat sink temperature of +60 °C; with the maximal heat transfer rate of 5 W and 16 W, respectively.

Both heat pipes have in common, that below the found transition point of −27 °C no rise of resistance is observed with increasing input power, and it decreases slightly approaching a constant value. When the heat sink temperature is above −20 °C, a first change of resistance can be found, for example for HP-A between 2 and 4 W. The first rise of the resistances is an indicator for reaching the capillary limitation. The deviation between calculated and measured limitation can have different sources. One is the calculation of the maximal capillary pressure with an uncertainty of 15 % [16]. It is found that for the capillary limitation the condenser temperature (approx. the same as the heat sink temperature) is the best reference. For the viscous limitation, the evaporator endcap temperature is the best reference, since this limitation is dependent on the maximal saturation pressure.

For temperatures above the transition point a sudden change in the resistance is observed. For temperatures below, it is not. For total heat pipe resistance, the resistance between adiabatic section and the condenser is dominant. The resistance

between the evaporator and adiabatic section does not change significantly. This behavior can be explained by a formation of a liquid slug in the condenser. The same test is conducted with a positive (condenser above evaporator) and a negative (condenser below evaporator) inclined heat pipe. The observation of the negative inclined heat pipe (see test results in chapter 5) reinforces this explanation as gravity benefits liquid flowback to the evaporator, increasing the capillary pressure limit and therefore enlarging the evaporator temperature.

5 RESULTS OF THERMAL CYCLING AND START-UP TESTS

5.1 Thermal Cycling Tests. During the thermal cycling test, the power input is hold constant and the sink temperature is suddenly lowered. The transient behavior is now examined, to identify the transition point from nearly isothermal to non-isothermal temperature profile of heat pipe shell (capillary limitation). This switching effect is a desirable feature to separate the evaporator from the condenser section. Figure 7 shows an example of a temperature cycle from +60 to −60 °C for HP-A.

The acting limitation is the capillary. For a heat input of 5 W, it is calculated to be at a sink temperature of about −11 °C. Additionally the change of resistance during the cycle is shown. At about 40 minutes the resistance begins to rise, at this point the heat pipe encounters the capillary heat transfer limit. The limiting sink temperature is identified in the test at about 5 °C. CFD analysis for this case shows, that the maximal velocity is at about **M** = 0.35. Therefore the starting point of the switching effect is not triggered by the sonic limitation. After this point, the temperature drops cause a higher pressure difference. As soon as this difference is high enough, the choked vapor flow

prevents propagation of a decreasing condenser temperature. This is indicated by a constant temperature at the boundary of the adiabatic section and the condenser, while the temperature in the condenser drops further, which is the typical behavior for this limitation. Additional test with a heat input Q_{in} of 10 W shows that the switching effect occurs near the calculated capillary limitation ($T_{\mathrm{sink}} \approx +20$ °C at $Q_{in} = 10$ W). This indicates that the capillary limitation is the cause of the first transition point. Another phenomenon can be observed at about 65 minutes, the evaporator begins to dry-out indicated by the temperature increase. This dry-out benefits the formation of a liquid slug in the condenser. In additional cycles ranging from +20 to −40 °C and +20 to −10 °C with the same heat input, the heat pipes show the same transition point as in Fig. 7, indicating that the switching point occurs at the same sink temperature and does not depend on the maximal cooling temperature. The heat pipes repeated their characteristics after being in essential overheating conditions at 20…40 °C in the evaporator.

Two main differences with Fig. 7 are observed at cycling between −20 and −70 °C with an applied power of 1 W. First the heat pipe does not encounter the capillary limitation and is in the viscous regime. The heat input is below the calculated transition power between the viscous and capillary limitation of 2.7±0.5 W (Fig. 4). Because the capillary limitation is not encountered, the governing temperature reference is at the evaporator. The switching effect is now at the transition temperature of about −27±2 °C at the evaporator endcap. And second, the temperature profile is different. The temperature in the adiabatic section is not uniform but drops linearly from the

evaporator to the condenser. CFD analysis for a sink temperature of −70 °C shows, that a temperature of −42 °C at the evaporator endcap is required to reach the sonic limitation. The evaporator temperature at steady-state is at about −34 °C, which means that the heat pipe is in the sonic limitation. But the temperature in the adiabatic section drops further contrary to the theory. This can be an effect of thermal conduction through the shell and wick of the heat pipe. The information of a colder condenser may not propagate backwards through the sonic vapor flow, but through the wick and shell. It seems that the heat transfer through the vapor with low density is not high enough to keep a constant temperature, as it is the case for higher heat inputs. In conclusion of the thermal cycling test, it can be concluded that the heat pipes are governed by the capillary limitation at high heat inputs. This limitation is the only one which determines the first transition point from nearly isothermal operation to non-isothermal condition. At lower heat inputs, the temperature drops further reaching the viscous limitation. This limitation defines the second transition point at low temperatures / heat inputs.

5.2 Start-up Tests. To verify the second transition point ($p_{\mathrm{sat}} = p_{c,\max}$ at −27±2 °C) various start up tests were made. During this test period the sink temperature is held constant and a sudden heat input above the calculated limitations is applied. The evolution of the temperature in the evaporator gives hints to the occurrence of heat transfer limitations. While at the thermal cycling test, the capillary limitation is firstly encountered for high heat inputs, it is the opposite for startup test. Because the heat pipes start at low temperatures, they go first through the viscous and sonic regime reaching the capillary limitation. The start at a sink temperature of about −60 °C with a

heat input of 5 W is shown in Fig. 8. The transition point between the capillary and viscous limitation is found to be at the calculated temperature.

When the evaporator reaches this transition point, the temperature profile changes along the heat pipe. A dry-out in the evaporator is indicated by the high temperature drop to the adiabatic section. In the adiabatic section the temperature becomes uniform and in the condenser the formation of the liquid slug is visible due to the temperature rise at the entrance and the constant temperature in the rest of condenser. The occurrence of the transition point is neither dependent on the heat input nor on the sink temperature. It solely depends on the temperature at the evaporator endcap, if it is at the temperature about −27 °C or not. The occurrence was tested for sink temperatures of −75 °C, −70 °C, −60 °C and −40 °C and for heat inputs of 5 W, 10 W and 15 W. While this effect is good visible for sink temperatures up to −60 °C, it is unclear for a sink temperature of −40 °C. The reason is the exponential nature of the saturation pressure of methanol. In conclusion of the startup tests, it can be said that the saturation and the maximal capillary pressure determine the point at low temperature, where the heat pipe switches and changes its temperature profile. During the heating, the heat pipe goes also through the sonic limitation. It is obvious, that these phenomena cannot be described with the viscous limitation as given in the literature (Eq. (2)). In the derivation of this limitation, the inertia forces are neglected, but the test shows, that this point is even reached when sonic vapor flow is present. This limitation is a rather a second pressure-based limit, as like the capillary limitation (Eq. (3)) and not the classical viscous limitation as described by Busse [12].

An additional test with inclined heat pipe was performed to verify the transition point hypothesis for $p_{\mathrm{sat}} = p_{c,\max}$. The inclination benefits the liquid flowback to the evaporator. This ensures that the capillary limit is raised due to gravity assistance. A higher maximal capillary pressure moves the transition point to higher temperatures. The new calculated transition point is at about −22±2 °C and is confirmed by the inclined heat pipe test.

This indicates that the hypothesis is correct and that another influence on the occurrence of this transition point can be excluded. The dry-out in the evaporator is also not as distinct as for the non-inclined heat pipe due to the beneficial flow back of working fluid to the evaporator.

6 HEAT PIPE OPERATION WITH HEAT OUTPUT BY RADIATION

6.1 The Thermal Vacuum Tests (TVAC) on a Subsystem Level. In the course of MASCOT TCS R&D activity the heat pipes operation was verified in one thermal vacuum test on the subsystem level and six thermal vacuum tests on the system level.

The start-up of the heat pipe from cold initial temperatures with high applied heat power had the most concerns. In [9] heat pipe start-up tests were performed with initial temperatures of −20 °C in the evaporator and −85 °C in the condenser with uncooled condensation section and an applied power of 10 W. These tests showed an essential rise of the evaporator temperature up to +80 °C with a temperature difference of 120 K along the heat pipe length. After the condenser and vapor temperatures reach −40 °C and 20 °C for HP-A (0 °C and +10 °C for HP-B), a normal evaporation–

condensation cycle started and the evaporator temperature decreased to +40 °C. No comment on such HP behavior is presented [9].

By considering the importance of such starting regimes at low initial temperature, a thermal mock-up of TCS system is designed (Fig. 9). The system consists of a heating source simulating the electronic box heat supply (heater 1), two heat transferring flanges, two heat pipes (HP-A and HP-B), an aluminum honeycomb radiator, mechanical supports and a thermal shroud.

Previously described 2D configured heat pipes were used, transferring heat from heater 1 to the radiator. Individual heaters A and B, installed on corresponding flanges are used for individual test of heat pipes. Mechanical supports are used to hold the heat pipes in a horizontal plane as they have individual deviation in shape.

The test run can be divided into four parts (Fig. 10). In part A, there is a temperature stabilization at the low heat input Q = 0.8 W. Part B is a preheating phase with a heater power of Q = 5.0 W. In parts C and D, the electronic box operation is simulated by a heat input of 9.3 W for each heat pipe. The temperature difference between the evaporator and the condenser is 32 K in part A and 11 K in part D, although the applied heater powers differ by eleven times. Variation of heat pipe thermal resistance reaches from 40 K/W to 1.1 K/W, correspondently. There no overheating of the heater has been observed. Different character of start-up [9] and current test is connected with the impact of heat capacity ratio $\varphi = C_E/(C_C + C_{\mathrm{rad}})$ on the evaporator overheating above steady state temperature. At the condition of the current

experiment at a value $\varphi > 2$ the overheating is not observed, at $\varphi < 1$ it reaches 5 K and more.

6.2 The Thermal Vacuum Tests on a System Level. The TCS works as a part of the MASCOT lander. The following phases are important: heat pipe operation in cruise hibernation with minimal applied power and lowest external fluxes on the radiator (Fig. 11). The radiator lays on temperature level −65…−35 °C, heat pipes reduce the heat transfer from the electronic box to the radiator, providing minimal power consumption from HY2. After preheating is completed, the initiation of the MASCOT electronic is foreseen. The heat pipe thermal resistance in cruise hibernation is larger than 20 K/W (at $T_{\mathrm{rad}} = -65$ °C), reducing its value to ~6 K/W in the preheating phase.

In the experimental simulation of the MASCOT operation on the asteroid surface, three variable values act on the TCS: the inner power generation, the asteroid soil temperature and the illumination on the lander sides and the main radiator (Fig. 12). The radiator temperature varies between −25 and +5 °C. The heat pipe thermal resistance is about 1.2 and 4 K/W during the Sun illumination period and during the night, respectively. The temperature of the evaporator lies inside −10…+10 °C, which provides the acceptable temperature conditions for the lander electronics.

6.3 Flight performance. After the launch of HY2 spacecraft, 11 sets of telemetric contacts took place. The heat pipe system has repetitively confirmed its ability to start from the high thermal resistance condition to the low one. MASCOT successfully landed on the asteroid and completed its program on October 3rd, 2018.

7 CONCLUSIONS

Methanol-copper heat pipes with fibrous capillary copper structure are characterized as a part of the MASCOT lander TCS. They have shown a change of their thermal resistance by two orders, as a function of the applied heat flux (0.25…10 W) and the heat sink temperature (−70…+60 °C). The performed study shows that such variable properties are the consequence of inner heat transfer process changes, taking place at passing the vapor sonic velocity limit, viscous limit and the capillary limit. A transition point for the condition $\Delta p_{c,\max} = p_{\mathrm{sat}}$ is found to be at about −27±2 °C in the evaporator. Below this point the heat pipes are in viscous limitation showing nearly isothermal temperature profiles in the evaporator and condenser with practically linear temperature drop in the adiabatic zone. For temperatures above the transition point the heat pipes are in capillary limitation with typical dry-out phenomenon in the evaporator shown by a temperature drop between the evaporator and the adiabatic section. After being in overheated conditions with a temperature difference between the evaporator and the condenser of 110 K, the heat pipes return in normal mode of operation as typical for conventional heat pipes. The heat pipes operation in the TCS of MASCOT lander, observed in ground thermal vacuum tests and in flight during 2014–2017, did not show deviations from expected performance of the thermal control system.

ACKNOWLEDGMENT

The authors acknowledge the contribution of the National Technical University of Ukraine “Kyiv Polytechnic Institute” for the fabrication of the studied heat pipes. The

reported work was performed at the German Aerospace Center (DLR) in Institute of Space Systems, under the projects “MASCOT” and “TCS design, Carbotherm”.

NOMENCLATURE

A_v	Vapor cross area, m^2
A_w	Wick cross area, m^2
C_C	Condenser heat capacity, J/K
C_E	Evaporator heat capacity, J/K
C_{rad}	Radiator heat capacity, J/K
d_s	Outer heat pipe diameter, m
d_v	Vapor space diameter, m
d_w	Inner heat pipe diameter, m
H_{fg}	Heat of vaporization, J/kg
K	Wick permeability, m^2
L_A	Adiabatic section length, m
L_C	Condenser section length, m
L_E	Evaporator section length, m
L_{Eff}	Effective heat pipe length, m
L_{HP}	Total heat pipe length, m
m_{HP}	Mass of heat pipe, kg
p	Pressure, N/m^2
p_{sat}	Saturation pressure, N/m^2

Q	Heat flux, W
R	Thermal resistance, K/W
r_v	Vapor space radius, m
T	Temperature, K or °C
T_{sink}	Sink temperature, °C
T_{Tr}	Transition temperature, °C
V_{wf}	Volume of working fluid, ml
ε	Wick porosity, -
λ	Thermal conductivity, W/(mK)
μ	Viscosity, Pa s
ρ	Density, kg/m^3
σ	Surface tension, N/m
φ	Heat capacity ratio, -
Kn	Knudsen number; (τ/d_v), where τ - the free mean path of molecule
M	Mach number; (u_v/c), where u_v – local vapor velocity, c- local sound velocity in vapor
We	Weber number; $(\rho_v u_v^2 l/\sigma)$, where l – characteristic dimension of pores of capillary structure

REFERENCES

[1] Watanabe, S., Tsuda, Y., Yoshikawa, M., Yoshikawa, M., Tanaka, S., Saiki, T., and Nakazawa, S., 2017, "Hayabusa2 Mission Overview," Space Science Reviews, Vol. **208**, Issue 1–4, pp. 3–16. DOI: 10.1007/s11214-017-0377-1.

[2] Jaumann, R., Schmitz, N., Koncz, A., Michaelis, H., Schroeder, S.E., Mottola, S., Trauthan, F., Hoffmann, H., Roatsch, T., Jobs, D., Kachlicki, J., Pforte, B., Terzer, R., Tschentscher, M., Weisse, S., Mueller, U., Perez-Prieto, L., Broll, B., Kruselburger, A., Ho, T.-M., Biele, J., Ulamec, S., Krause, C., Grott, M., Bibring, J.-P., Watanabe, S., Sugita, S., Okada, T., Yoshikawa, M., and Yabuta, H., 2017, "The Camera of the MASCOT Asteroid Lander on Board Hayabusa," Space Science Reviews, Vol. **208**, Issue 1–4, pp.375–400. DOI: 10.1007/s11214-016-0263-2.

[3] Bibring, J.-P., Hamm, V., Langevin, Y., Pilorget, C., Arondel, A., Bouzit, M., Chaigneau, M., Crane, B., Darié, A., Evesque, C., Hansotte, J., Gardien, V., Gonnod, L., Leclech, J.-C., Meslier, L., Redon, T., Tamiatto, C., Tosti, S., and Thoores, N., 2017, "The MicrOmega Investigation Onboard Hayabusa2," Space Science Reviews, Vol. **208**, Issue 1–4, pp. 401–412. DOI: 10.1007/s11214–017–0335–y.

[4] Hercik, D., Auster, H.-U., Blum, J., Fornaçon, K.-H., Fujimoto, M., Gebauer, K., Güttler, C., Hillenmaier, O., Hördt, A., Liebert, E., Matsuoka, A., Nomura, R., Richter, I., Stoll, B., Weiss, B.P., and Glassmeier, K.-H., 2017, "The MASCOT Magnetometer," Space Science Reviews, Vol. **208**, Issue 1–4, pp. 433–449. DOI: 10.1007/s11214-016-0236-5.

[5] Grott, M., Knollenberg, J., Borgs, B., Hänschke, F., Kessler, E., Helbert, J., Maturilli, A., and Müller, N., 2017, "The MASCOT Radiometer MARA for the Hayabusa 2 Mission," Space Science Reviews, Vol. **208**, Issue 1–4, pp. 412–431. DOI: 10.1007/s11214–016–0272–1.

[6] Celotti, L., Solyga, M., Nadalini, R., Kravets, V., Khairnasov, S., Baturkin, V., Lange, C., Findlay, R., Ziach, C., and Ho, T., 2015, "MASCOT thermal subsystem design challenges and solution for contrasting requirements," *Proceedings of 45th International Conference on Environmental Systems*, Bellevue, Washington, July 12–16, 2015, Report ICES–2015–83. URI: http://hdl.handle.net/2346/64366.

[7] Baturkin, V., Zhuik, S., and Savina, V., 1990, "Development and research of heat pipes for thermal control system of scientific apparatus," *Proceedings of IV international seminar "Scientific Space Instrumentation"*, t. Frunze, USSR, September 18-24, 1989", Institute of space research, USSR Academy of sciences, Vol. **IV**, pp. 201–208.

[8] Baturkin, V., Zhuk, S., Vojta, J., Lura, F., Biering, B., and Lotzke, H.G., 2003, "Elaboration of thermal control systems on heat pipes for microsatellites Magion 4, 5

and BIRD," Applied Thermal Engineering, Vol. **23**, pp. 1109–1117. DOI: 10.1016/S1359–4311(03)00040–1.

[9] Kravets, V., Alekseik, Y., Alekseik, O., Khairnasov, S., Baturkin, V., Ho, T., and Celotti, L., 2016, "Heat pipes with variable thermal conductance property developed for space applications," Journal of Mechanical Science and Technology, **31**(6), pp. 2613–2620. DOI: 10.1007/s12206–017–0503–8.

[10] Faghri, A., 2016, Heat Pipe Science and Technology, Second Edition, Global Digital Press, ISBN: 978–0–9842760–1–1.

[11] Semena, M.G., 1979, "Method of computing the thermal resistance of low-temperature heat pipes with metal-fiber wicks," Journal of Engineering Physics, Vol. **36**, Issue 3, pp. 287–292. DOI: 10.1007/BF00861912.

[12] Busse, C.A., 1973, "Theory of the ultimate heat transfer limit of cylindrical heat pipes," International Journal of Heat and Mass Transfer, Vol. **16**, Issue 1, pp. 169–186. DOI: 10.1016/0017–9310(73)90260–3.

[13] Kemme, J.E., 1969, "Ultimate heat-pipe performance," IEEE Transactions on Electron Devices, Vol **16**, Issue 8, pp. 717–723. DOI: 10.1109/T–ED.1969.16845.

[14] Levy, E.K., 1968, "Theoretical Investigation of Heat Pipes Operating at Low Vapor Pressures," Journal of Engineering for Industry, **90**(4), pp. 547–552. DOI: 10.1115/1.3604687.

[15] Bertossi, R., Romestant, C., Ayel, V., and Bertin, Y., 2012, "Theoretical study and review on the operational limitations due to vapor flow in heat pipes," Frontiers in Heat Pipes, 3–023001. DOI: 10.5098/fhp.v3.2.3001.

[16] Semena, M.G., and Gershuni, A., 1981, "Analysis of the capillary-transport characteristics of metal-fiber structures," Journal of Engineering Physics, Vol. **41**, Issue 1, pp. 683–688. DOI: 10.1007/BF00824808.

[17] Kim, B. H., and Peterson, G.P., 1995, "Analysis of the critical Weber number at the onset of liquid entrainment in capillary-driven heat pipes," International Journal of Heat and Mass Transfer, Volume **38**, Issue 8, pp. 1427–1442. DOI: 10.1016/0017–9310(94)00249–U.

[18] Kim, B. H., and Peterson, G.P., 1994 "Theoretical and physical interpretation of entrainment phenomenon in capillary-driven heat pipes using hydrodynamic instability theories," International Journal of Heat and Mass Transfer, Vol. **37**, Issue 17, pp. 2647–2660. DOI: 10.1016/0017–9310(94)90382–4.

Figure Captions List

Fig. 1 The main components of the MASCOT lander and its TCS components. The MESS structure is used for attaching the lander to HY2 and stays (together with MESS MLI) as part of HY2 after the lander's separation. The surfaces with specified optical properties, external cables, and some equipment are not shown.

Fig. 2 The configuration of 2D heat pipes used: a - heat pipe HP-A; b - heat pipe HP-B; c - cross-section in evaporator, adiabatic and condenser with components; 1 - location of evaporator cap; 2 - location of condenser cap; 3 - plane for heater attachment; 4 - plane for condenser block attachment; 5 - soldering of heat pipe shell and flange

Fig. 3 Heat transfer limitations of heat pipes at different operating temperatures [10]

Fig. 4 Calculated heat transfer limitations of heat pipe HP-A. Heat pipe HP-B is similar.

Fig. 5 General test setup in the thermal vacuum chamber: 1 - heat pipe; 2 - condenser block; 3 - evaporator stand; 4 - thermal insulation; 5 - copper shroud with SLI cover; 6 - MLI cover around shroud; 7 - alignment screws; 8 - mounting plate (heat sink); 9 - interfaces between thermal vacuum chamber and laboratory; 10 - wagon (aluminum profile); 11 - rolls; 12 - rail; 13 - cooling hose

Fig. 6 Thermal resistance for HP-A at different heat sink temperatures. Similar to that of HP-B. Resistance is calculated by dividing the temperature difference between the mean evaporator temperature and the mean condenser temperature by the applied power.

Fig. 7 Thermal cycling of HP-A at a constant heat input of 5 W from +60 °C to −60 °C and change of thermal resistance during sink cooling. Similar behavior for HP-B is observed.

Fig. 8 The temperature variation with respect to the time by starting at a sink temperature of about −60 °C and a heat input of 5 W for HP-A

Fig. 9 Scheme of thermal mock-up of TCS for autonomous test of MASCOT 2D heat pipes. Protection shrouds, MLI, montage plate are not shown.

Fig. 10 Heat pipe HP-B start-up from cold conditions: sensors E1, E2 - evaporator, sensors A1, A2 - adiabatic section, sensors C1, C2 - condenser, sensors R1, R2 - radiator. Location of sensors is in Fig. 9.

Fig. 11 Heat pipes operation in TVAC in cruise (hibernation and preheating)

Fig. 12 Heat pipes temperatures in TVAC during on asteroid soil operation (one of the nominal cases): Power to Radiator - re-calculated heat power, absorbed by the radiator coating from external light sources (sun, albedo and IR radiation of the asteroid)

Table Caption List

Table 1 Characteristics of investigated heat pipes

Property	HP-A	HP-B
Working fluid	Methanol	
Shell / Wick	Copper	
Wick type	Sintered metal fibers	
d_s	0.006 m	
d_v	0.0031 m	
d_w	0.005 m	
K	9.36×10^{-10} m²	
ε	0.82 to 0.84	
V_{wf}	6 ml	5 ml
L_A	0.259 m	0.256 m
L_C	0.127 m	0.083 m
L_E	0.096 m	0.099 m
L_{Eff}	0.3705 m	0.347 m
L_{HP}	0.482 m	0.438 m
m_{HP}	0.123 kg	0.112 kg

Table 2 Coefficients of thermophysical properties of methanol calculated with Eq. (1) given in SI units

	A_0	$A_1 T_r$	$A_2 T_r^2$	$A_3 T_r^3$
λ_l	0.300823	−0.176481	0	0
λ_v	−0.012552	0.112281	−0.205586	0.161913
ρ_l	1069.444	−486.028	0	0
$10^6 \mu_v$	−0.294716	17.11866	0	0
$10^{-6} H_{fg}$	1.710327	−2.163057	3.979509	−3.192026
σ	0.055371	−0.066307	0.017467	0
Property	A_0	$A_1 T_r^{-1}$	$A_2 T_r^{-2}$	$A_3 T_r^{-3}$
$\ln(\rho_v)$	11.44934	−6.593777	−0.550823	0
$\ln(\mu_l)$	−12.15963	2.868341	−0.095127	0
$\ln(p_{\mathrm{sat}})$	−23.94323	−7.513269	−0.43977	0

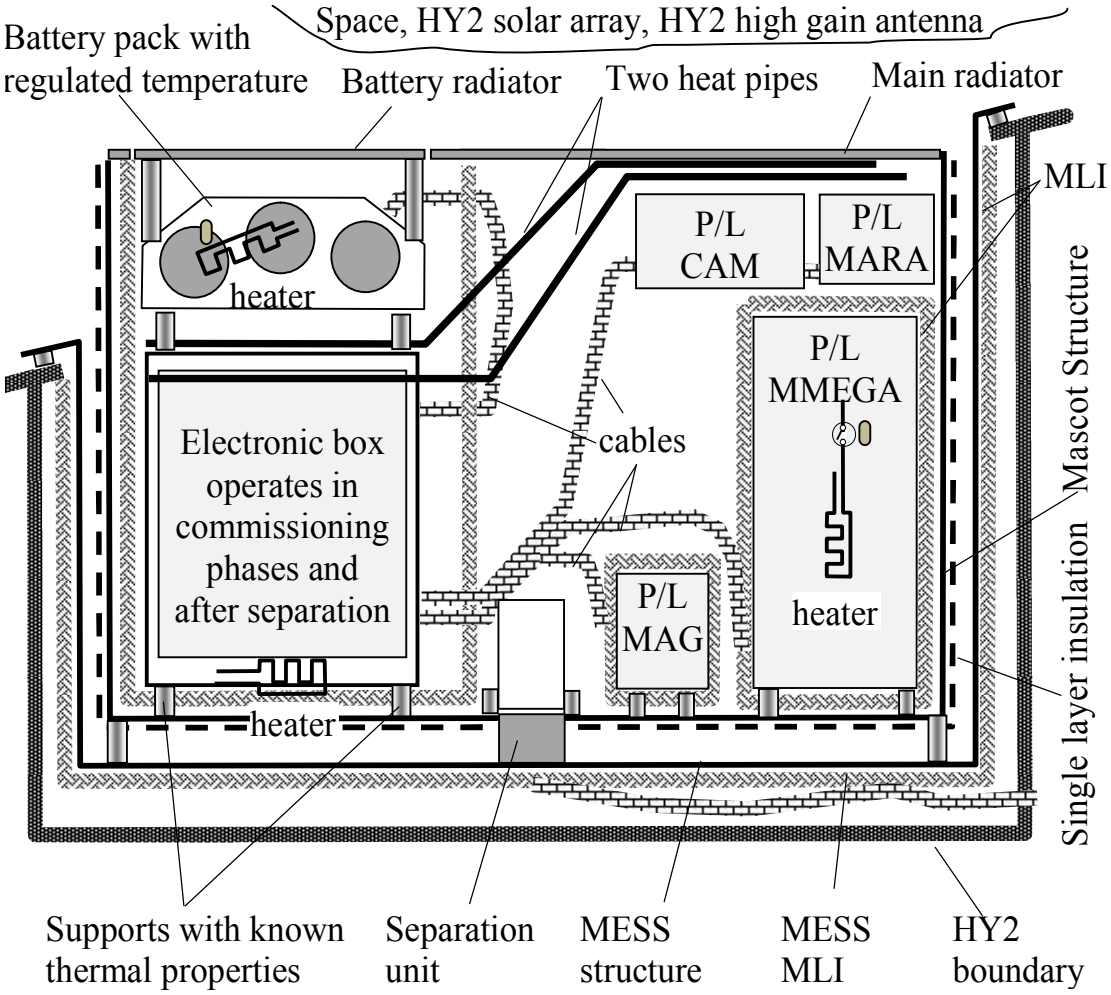

Fig. 1 The main components of the MASCOT lander and its TCS components. The MESS structure is used for attaching the lander to HY2 and stays (together with MESS MLI) as part of HY2 after the lander's separation. The surfaces with specified optical properties, external cables, and some equipment are not shown.

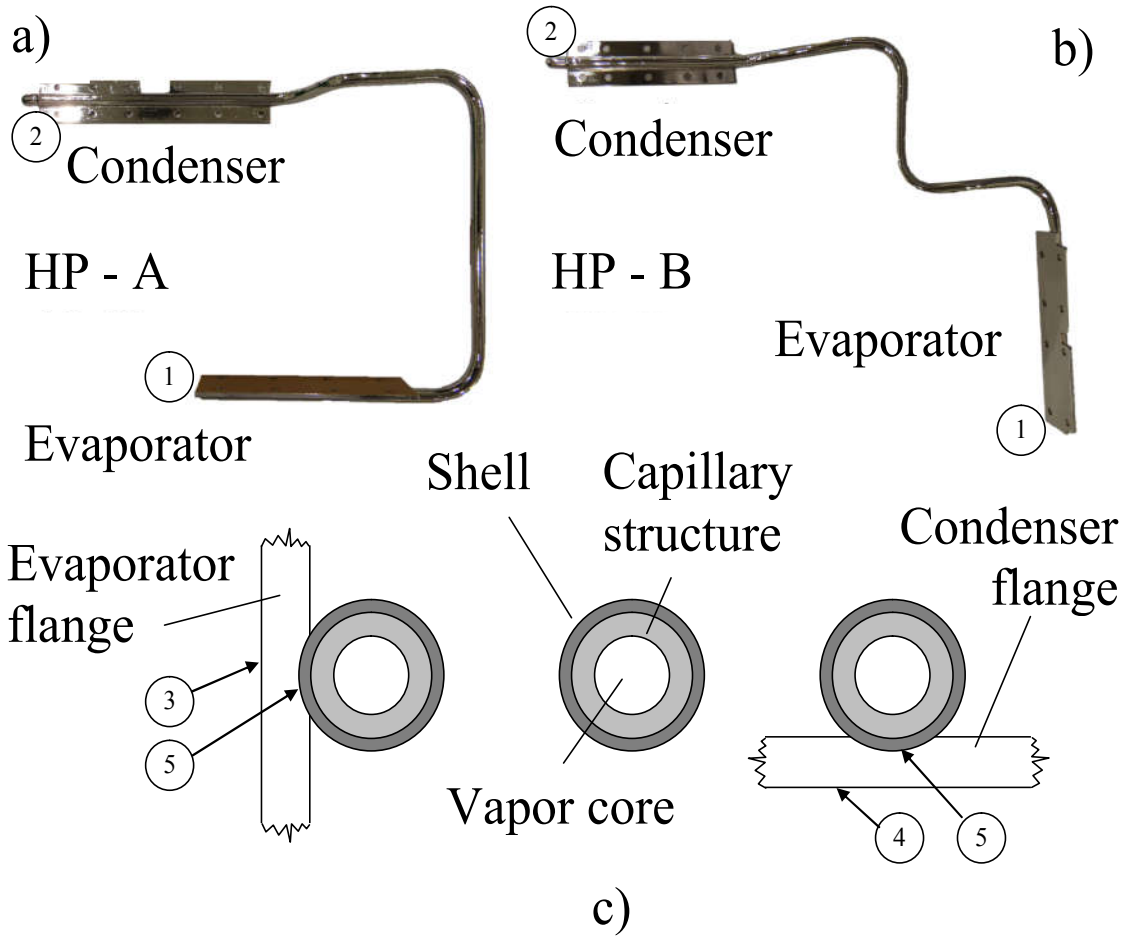

Fig. 2 The configuration of 2D heat pipes used: a - heat pipe HP-A; b - heat pipe HP-B; c - cross-section in evaporator, adiabatic and condenser with components; 1 - location of evaporator cap; 2 - location of condenser cap; 3 - plane for heater attachment; 4 - plane for condenser block attachment; 5 - soldering of heat pipe shell and flange

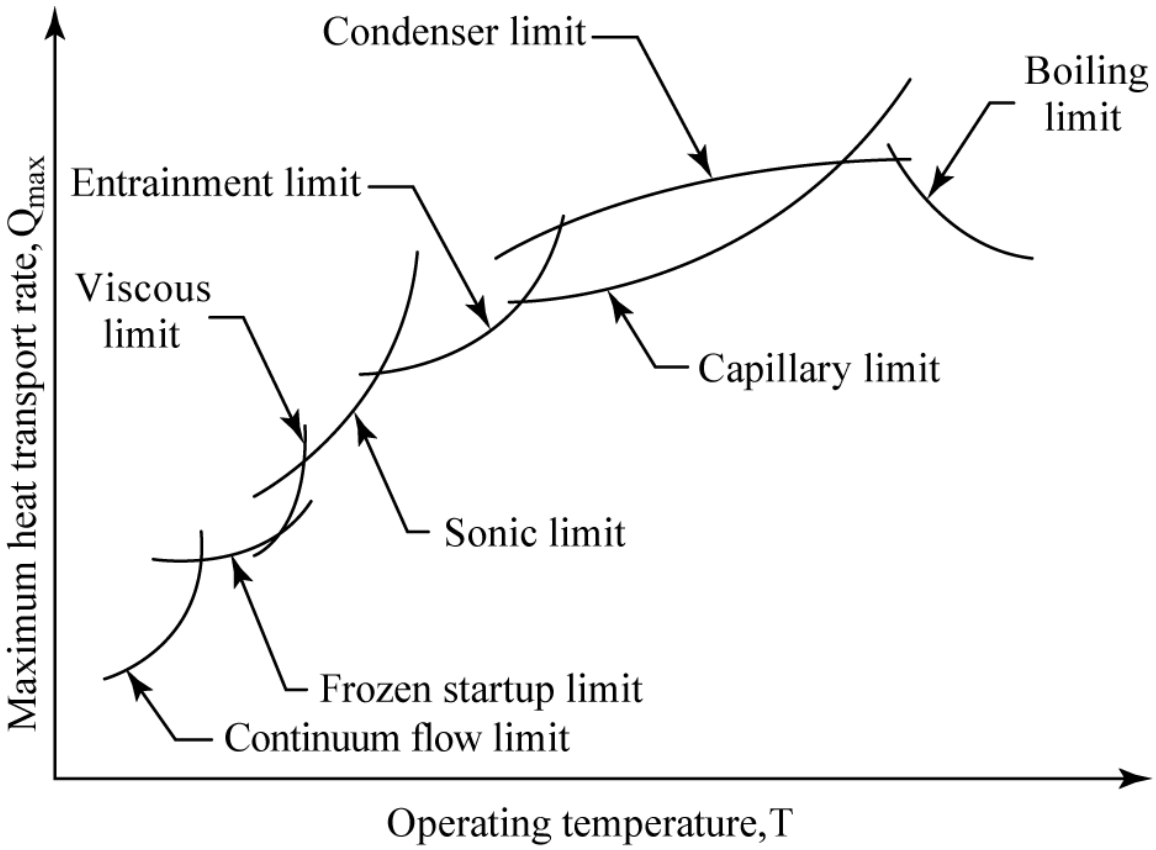

Fig. 3 Heat transfer limitations of heat pipes at different operating temperatures [10]

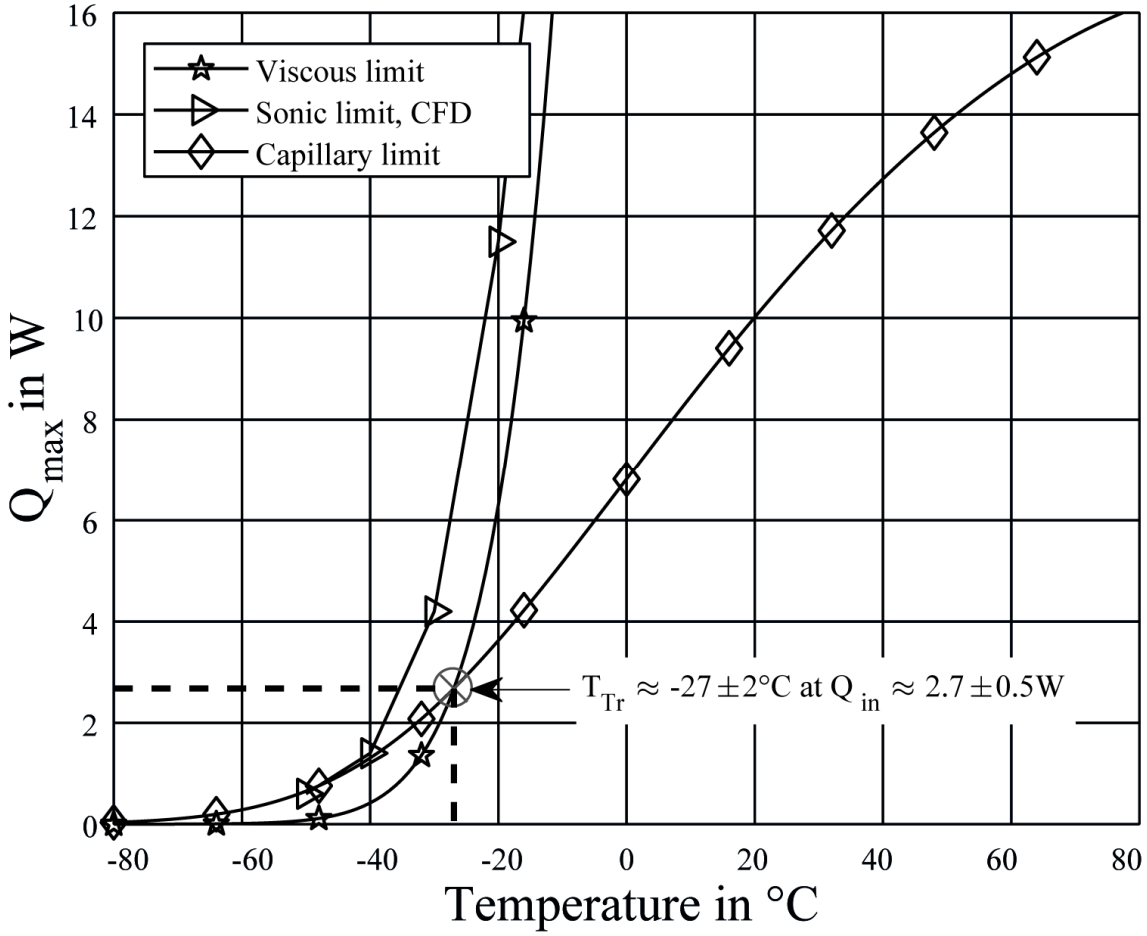

Fig. 4 Calculated heat transfer limitations of heat pipe HP-A. Heat pipe HP-B is similar.

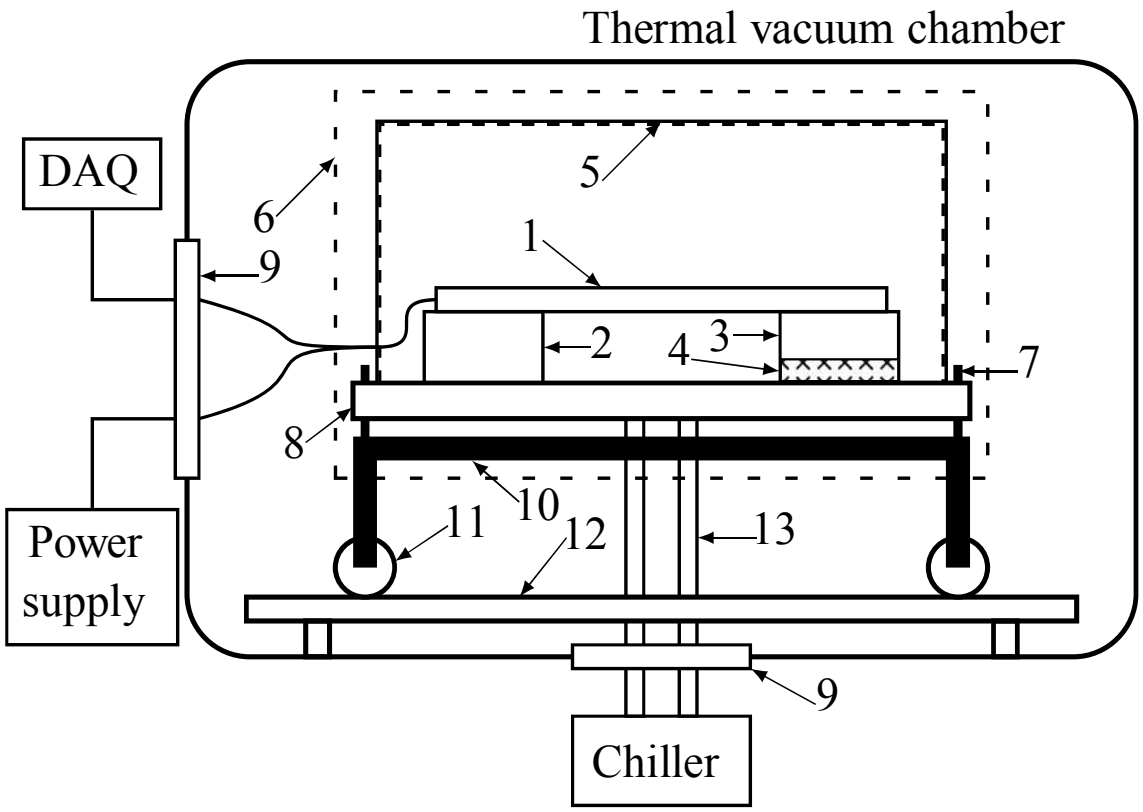

Fig. 5 General test setup in the thermal vacuum chamber: 1 - heat pipe; 2 - condenser block; 3 - evaporator stand with heater; 4 - thermal insulation; 5 - copper shroud with SLI cover; 6 - MLI cover around shroud; 7 - alignment screws; 8 - mounting plate (heat sink); 9 - interfaces between thermal vacuum chamber and laboratory; 10 - wagon (aluminum profile); 11 - rolls; 12 - rail; 13 - cooling hose

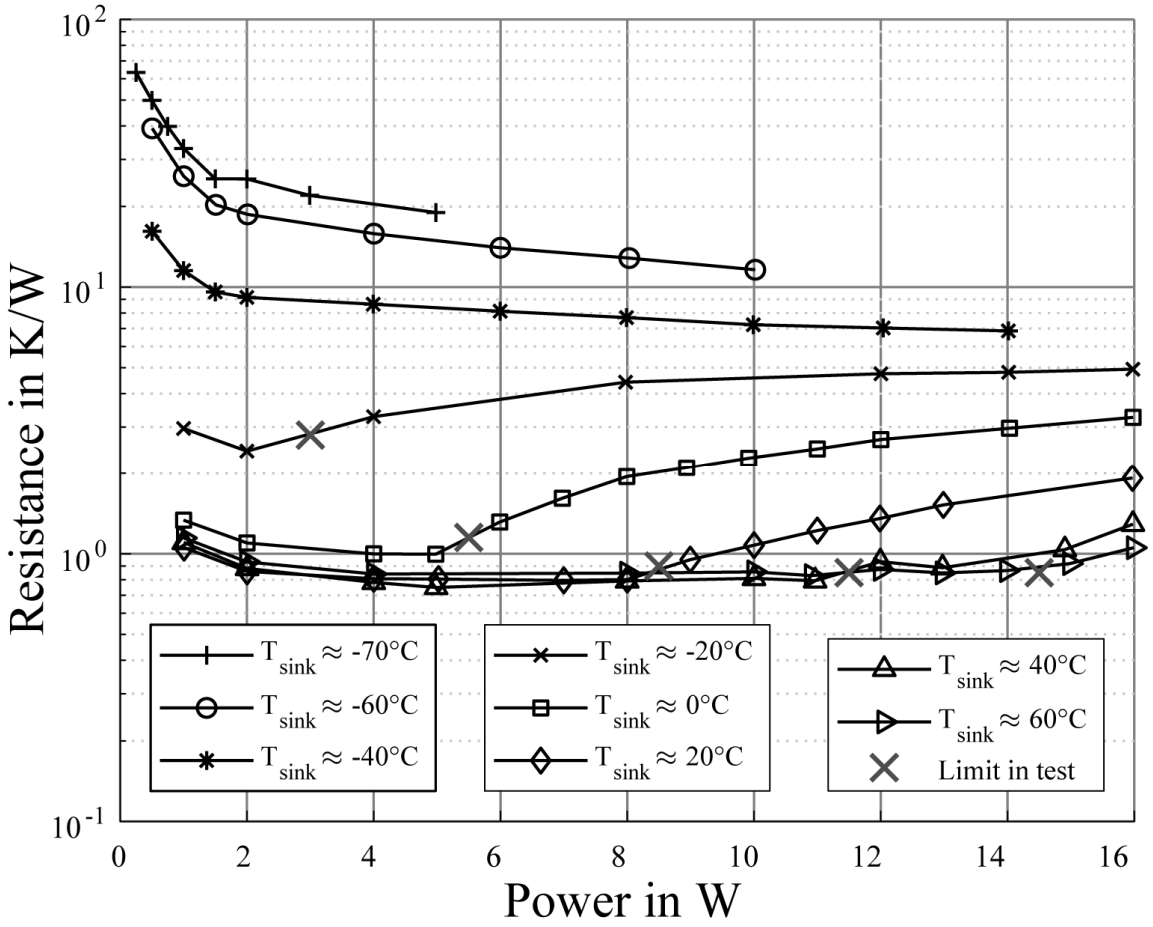

Fig. 6 Thermal resistance for HP-A at different heat sink temperatures. Similar to that of HP-B. Resistance is calculated by dividing the temperature difference between the mean evaporator temperature and the mean condenser temperature by the applied power.

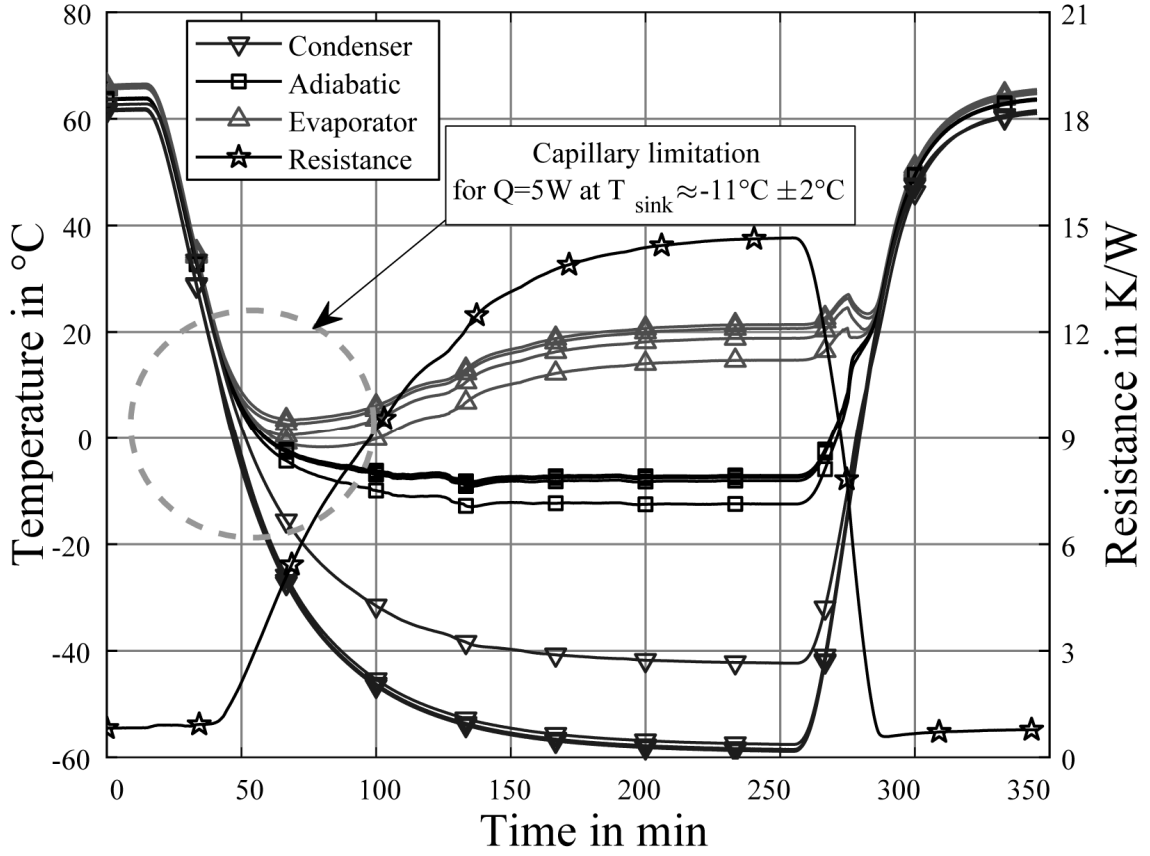

Fig. 7 Thermal cycling of HP-A at a constant heat input of 5 W from +60 °C to −60 °C and change of thermal resistance during sink cooling. Similar behavior for HP-B is observed.

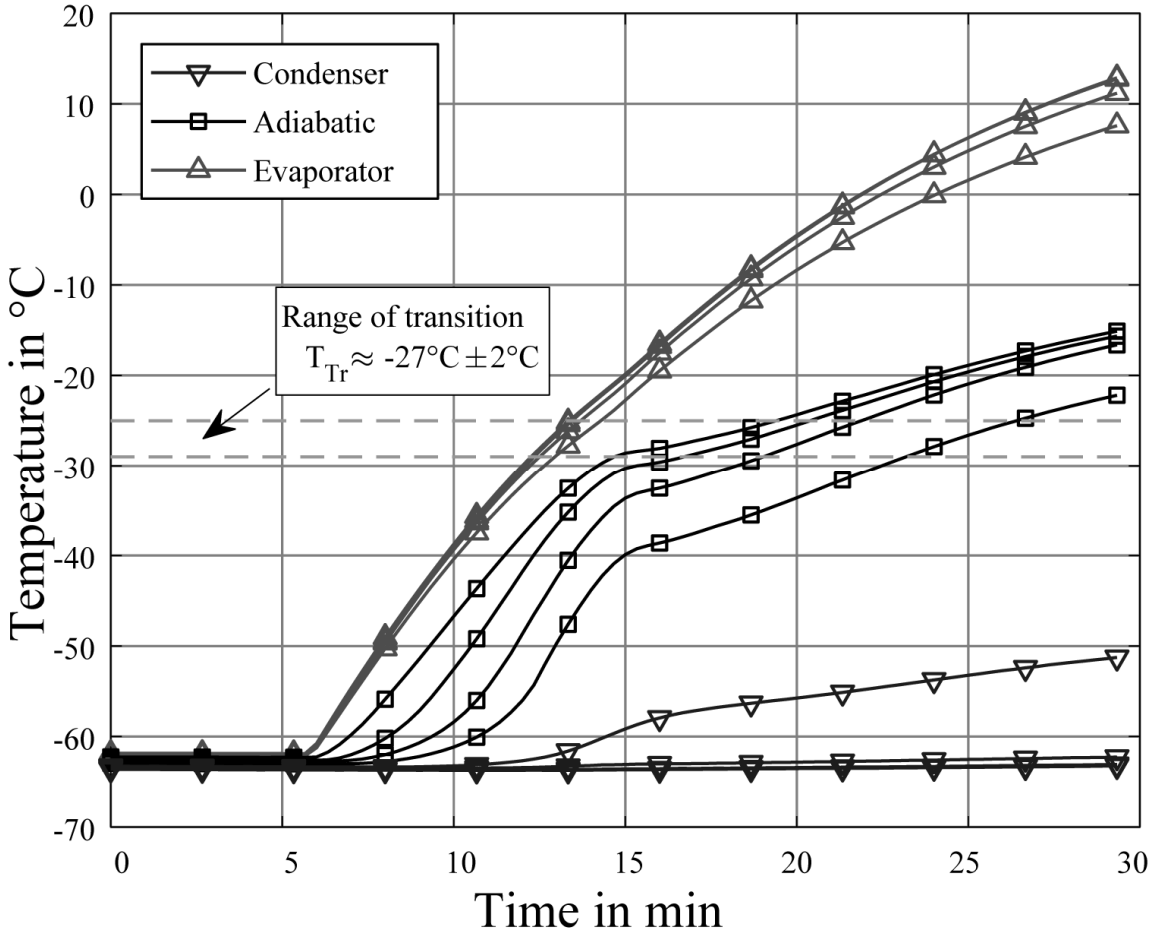

Fig. 8 The temperature variation with respect to the time by starting at a sink temperature of about −60 °C and a heat input of 5 W for HP-A

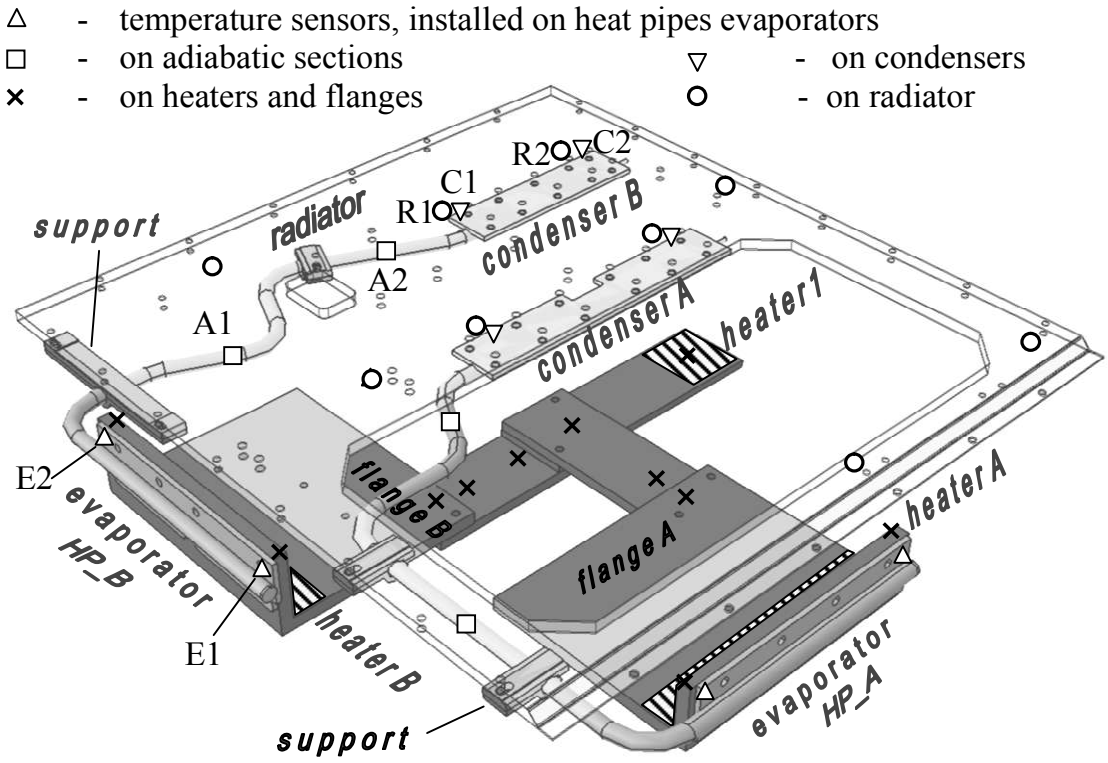

Fig. 9 Scheme of thermal mock-up of TCS for autonomous test of MASCOT 2D heat pipes. Protection shrouds, MLI, montage plate are not shown.

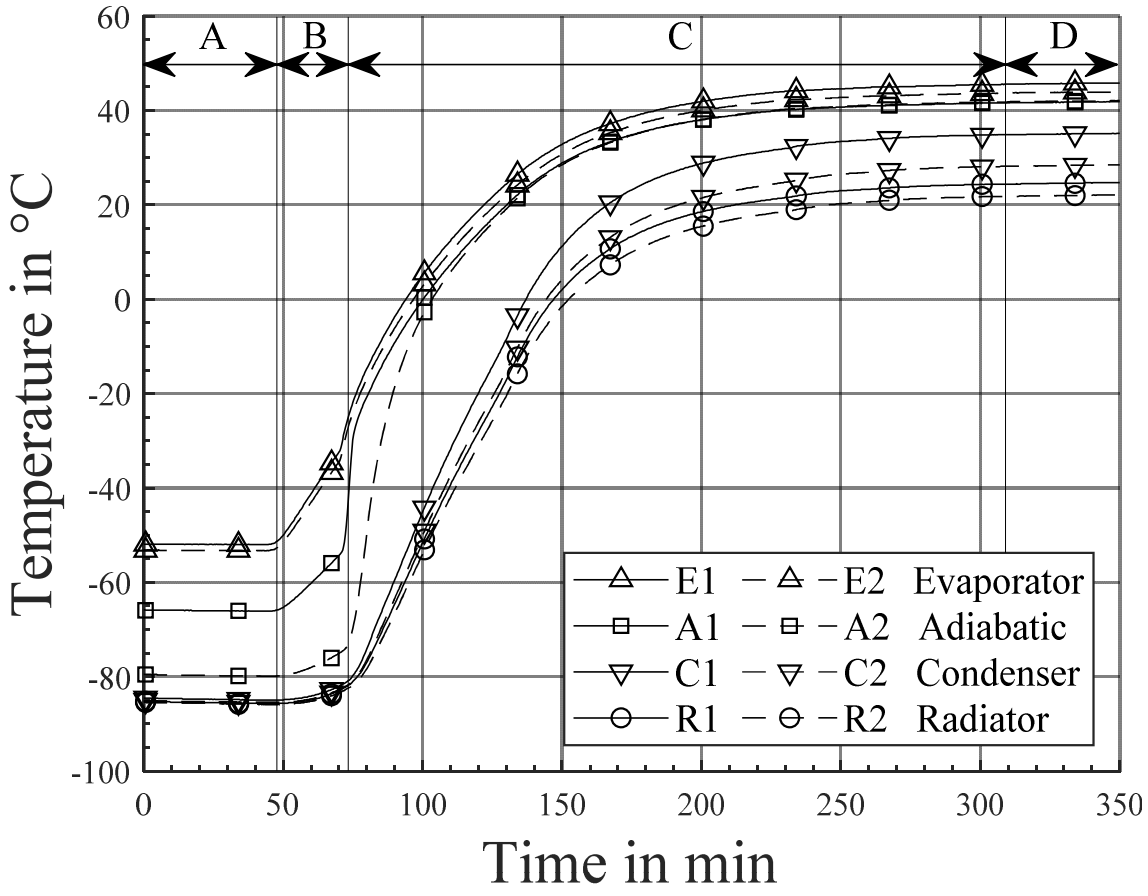

Fig. 10 Heat pipe HP-B start-up from cold conditions: sensors E1, E2 - evaporator, sensors A1, A2 - adiabatic section, sensors C1, C2 - condenser, sensors R1, R2 - radiator. Location of sensors is in Fig. 9.

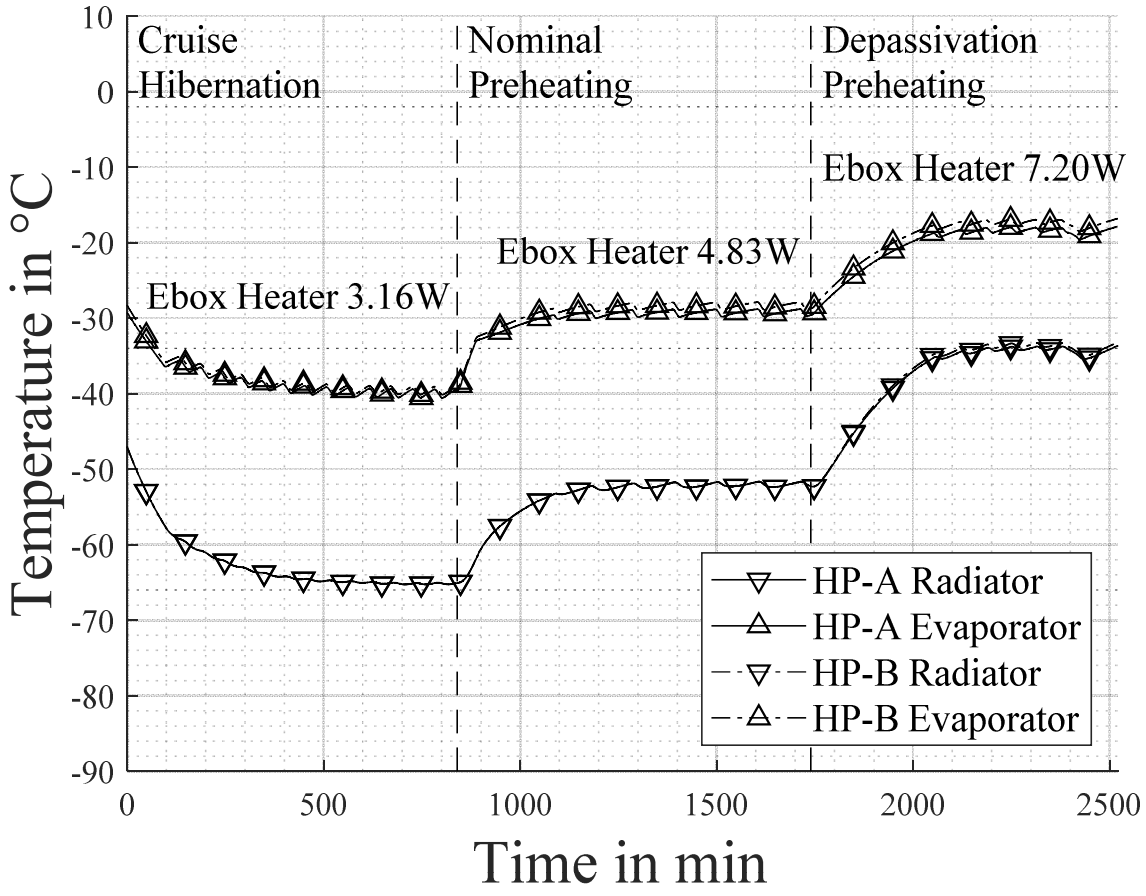

Fig. 11 Heat pipes operation in TVAC in cruise (hibernation and preheating)

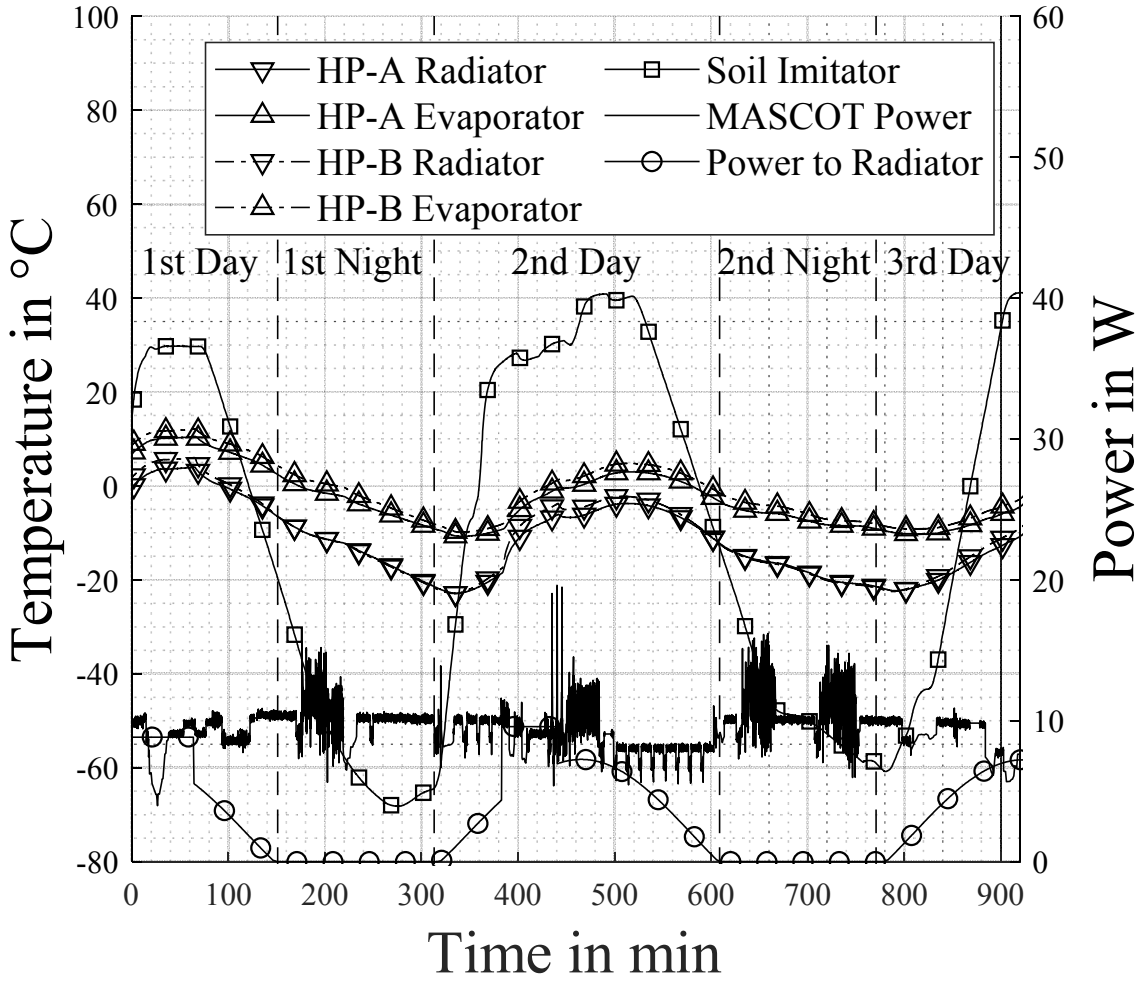

Fig. 12 Heat pipes temperatures in TVAC during on asteroid soil operation (one of the nominal cases): Power to Radiator - re-calculated heat power, absorbed by the radiator coating from external light sources (sun, albedo and IR radiation of the asteroid)